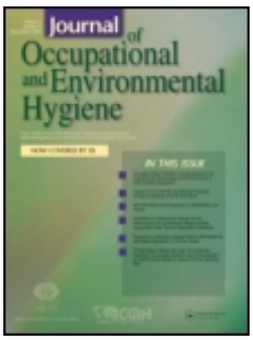

Journal of Occupational and Environmental Hygiene

ISSN: 1545-9624 (Print) 1545-9632 (Online) Journal homepage: http://www.tandfonline.com/loi/uoeh20

Comparison of Free Radical Generation by Pre- and Post-Sintered Cemented Carbide Particles

Aleksandr B. Stefaniak , Christopher J. Harvey , Valerie C. Bukowski & Stephen S. Leonard

To cite this article: Aleksandr B. Stefaniak , Christopher J. Harvey , Valerie C. Bukowski & Stephen S. Leonard (2009) Comparison of Free Radical Generation by Pre- and Post-Sintered Cemented Carbide Particles, Journal of Occupational and Environmental Hygiene, 7:1, 23-34, DOI: 10.1080/15459620903349073

To link to this article: http://dx.doi.org/10.1080/15459620903349073

Published online: 10 Nov 2009.

Journal of Occupational and Environmental Hygiene, 7: 23–34
ISSN: 1545-9624 print / 1545-9632 online
DOI: 10.1080/15459620903349073

Comparison of Free Radical Generation by Pre- and Post-Sintered Cemented Carbide Particles

Aleksandr B. Stefaniak, Christopher J. Harvey, Valerie C. Bukowski, and Stephen S. Leonard

National Institute for Occupational Safety and Health, Morgantown, West Virginia

Rapid generation of reactive oxygen species (ROS) may occur in response to cellular contact with metal particles. Generation of ROS by cobalt and/or tungsten carbide is implicated in causing hard metal lung disease (HMD) and allergic contact dermatitis (ACD). In this study, ROS generation and particle properties that influence radical generation were assessed for three sizes of tungsten, tungsten carbide, cobalt, admixture (tungsten carbide and cobalt powders), spray dryer, and post-sintered chamfer grinder powders using chemical (H_2O_2 plus phosphate buffered saline, artificial lung surfactant, or artificial sweat) and cellular (RAW 264.7 mouse peritoneal monocytes plus artificial lung surfactant) reaction systems. For a given material, on a mass basis, hydroxyl ($^{\cdot}OH$) generation generally increased as particle size decreased; however, on a surface area basis, radical generation levels were more, but not completely, similar. Chamfer grinder powder, polycrystalline aggregates of tungsten carbide in a metallic cobalt matrix, generated the highest levels of $^{\cdot}OH$ radicals ($p < 0.05$). Radical generation was not dependent on the masses of metals, rather, it involved surface-chemistry-mediated reactions that were limited to a biologically active fraction of the total available surface area of each material. Improved understanding of particle surface chemistry elucidated the importance of biologically active surface area in generation of ROS by particle mixtures.

Keywords dermal exposure, hard metal, inhalation exposure, particle physicochemical properties, reactive oxygen species

Address correspondence to: Stephen S. Leonard, Mail Stop 2015, 1095 Willowdale Road, Morgantown, WV 26505; e-mail: SLeonard@cdc.gov.

The findings and conclusions in this report are those of the authors and do not necessarily represent the views of the National Institute for Occupational Safety and Health.

INTRODUCTION

Cemented tungsten carbides (CTC) are wear-resistant alloys that contain tungsten carbide bound in a matrix of cobalt. Applications of cemented tungsten carbides include cutting tools for metals and drills for masonry, concrete, coal, and rock.[1] Inhalation of dusts generated during production of cemented tungsten carbides is associated with hard metal lung disease (HMD) among workers exposed to pre- and post-sintered dusts.[2–7] Skin exposure to cobalt is frequently associated with development of allergic contact dermatitis (ACD).[8]

To make cemented carbide alloys, tungsten metal powder and carbon black are milled and carburized (heat treated) to form tungsten carbide powder. Tungsten carbide powder is mixed with cobalt binder and additives (tantalum carbide, etc.), suspended in solvent, milled, dispersed in a spray dryer, and screened to form a (pre-sintered) powder that is compacted by pressing or extrusion to achieve a desired shape. Compacted material is sintered (heated until the cobalt binder phase becomes liquid; on cooling, the tungsten carbide grains become embedded in the binder) to form CTC. During sintering, the compacts shrink, necessitating grinding of the post-sintered shape to precise final dimension.

The generation of reactive oxygen species (ROS) by metal-containing particles and the resulting effects on cell signaling appear to result from a common mechanism: a respiratory or oxidative burst response to cellular contact with a foreign body.[9–15] One of the important members of the ROS family is the superoxide anion radical ($O_2^{\cdot -}$), which can be dismutated to form hydrogen peroxide (H_2O_2), and the highly reactive hydroxyl radical ($^{\cdot}OH$) in the presence of certain transition metal ions.[16,17] Generation of ROS may lead to the stimulation of inflammatory processes involving secretion of chemotactic factors, growth factors, proteolytic enzymes, lipoxygenases, cycloxygenase, inactivation of antiproteolytic enzymes, and the release of signaling proteins.[9–16] There is a critical balance between oxidants and antioxidant defenses.[18] When cells are unable to maintain this redox balance, it results in a chronic inflammatory state. This inflammatory state may result in damage to the cells involved and to the surrounding tissue due to activation of signaling pathways, inflammatory cytokine production, altered gene expression, and other cellular modifications. One of the most important mechanisms of metal-mediated free radical generation is via a Fenton-type reaction.[19] In this reaction the transition metal

ion reacts with H_2O_2 to generate $\cdot OH$ radical and an oxidized metal ion:

$$Metal^{n+} + H_2O_2 \rightarrow Metal^{n+1} + \cdot OH + OH^- \quad \textbf{(1)}$$

Using pre-sintered hard metal dusts, investigators have demonstrated that on a mass basis, ROS generation was greater for cobalt in the presence of tungsten carbide relative to the individual constituents alone,[20,21] which is consistent with the known catalytic properties of tungsten carbide.[22] Based on their data, these investigators hypothesized that when tungsten carbide and cobalt particles came into contact, cobalt was oxidized and electrons were transferred to the surface of the tungsten carbide particles, which reduced oxygen and generated ROS responsible for HMD.[20]

The exact mechanism by which cobalt causes ACD is not fully agreed upon. Cobalt ions may bind covalently with nucleophilic proteins to form hapten, which interacts with immunologically active layers of the skin to promote sensitization and elicitation of contact hypersensitivity via a T-lymphocyte cell-mediated reaction.[23–25] Rather than covalent bonding, Van de Broeke et al.[26] hypothesize that cobalt-ion-mediated redox reactions generate radicals that react with biological molecules in close proximity, thereby leading to formation of antigenic structural modifications in biological molecules and causing ACD.

Stefaniak et al.[27] characterized airborne particles generated during the production of cemented tungsten carbides and noted that elemental composition of the individual particles became increasingly heterogeneous with processing: mostly discrete cobalt- or tungsten-containing particles (prior to spray drying), then heterogeneous tungsten- and cobalt-containing particles (all subsequent work areas). A follow-on study of personal exposures revealed respirable size cobalt- and tungsten-containing particles in all work areas that span the production of cemented tungsten carbides.[28] Day et al.[29] evaluated dermal exposures of employees engaged in the manufacture of cemented tungsten carbides and reported substantial cobalt contamination on workers' hands and necks.

The biological activity of inhaled particles will depend on the physicochemical parameters of the material. Particle surface characteristics are key factors in the generation of ROS by many materials and also in the development of fibrosis, e.g., crystalline silica.[30] As such, Oberdörster et al.[31] recommend that when evaluating the toxicity of airborne particles, it is necessary to characterize particle size, shape, crystal structure, chemical composition (bulk and surface), and surface area. The powders used in the seminal studies by Lison et al.[20] yielded a mechanistic model; however, additional studies are needed to more fully investigate the role of particle size, crystal structure, chemical composition, and surface area to better understand the role of particle properties in the generation of ROS by cemented carbide powders.

The major goal of this study was to build on previous work by Lison et al.[20] and elucidate the influence of specific properties (size, surface area, chemistry) of real-world particles on ROS generation. Specifically, we evaluated ROS generation by various biologically relevant sizes of well-characterized, workplace-sampled powders in a series of in vitro tests, beginning with cell-free tests to understand production of free radicals by particles that contact lung and skin fluids, and progressing to a cellular test to provide information on production of free radicals by particles that interact with lung cells. An improved understanding of particle properties involved in generation of ROS would enable development of biologically meaningful exposure metrics for use in workplace exposure monitoring and health protection.

MATERIALS AND METHODS

Study Powders

Five representative metal powders that span the spectrum of powders used in the manufacture of cemented tungsten carbides were chosen for study. These powders were collected as bulk samples from containers of manufacturer feedstock powders (tungsten metal, tungsten carbide, and cobalt), a container of wet-milled and spray dried pre-sintered powder, and from the dust collector of a chamfer grinder used for final machining of post-sintered CTC product. Characterization of these powders demonstrated that the morphology and chemistry of the bulk materials are qualitatively similar to airborne particles to which workers are potentially exposed throughout the production of cemented tungsten carbides.[27]

A sixth material was prepared as an admixture by mechanically blending the aerodynamically size-separated (described below) tungsten carbide and cobalt powders at a ratio of 94:6 by mass to match common industrial grade powder.[32] The admixture is not an actual industrial powder but, instead, a mechanical mixture of feedstock powders prepared for the purpose of comparing free radical generation of loosely associated cobalt and tungsten carbide particles to the individual powders.

Aerodynamic Size Separation of Study Powders

Each bulk powder was aerodynamically size-separated in the laboratory using a dry powder disperser (Model 175; DeVilbiss, Somerset, Pa.) and five-stage aerosol cyclone[33] operated at 10 L/min as previously described.[34] The 50% aerodynamic cutoff diameters (D_{50}) of the aerosol cyclone were >10, 4.3, 2.9, 2.0, and 1.2 μm for stages 1 to 5, respectively. For the purposes of this study, we evaluated free radical generation by the materials collected in Stages 1, 2, and 3 of the aerosol cyclone. Material collected in Stage 1 ($D_{50} > 10$ μm) have particle sizes capable of penetrating into the conduction airways, i.e., thoracic-sized particles. Materials collected in Stage 2 ($D_{50} = 4.3$ μm) and Stage 3 ($D_{50} = 2.9$ μm) have particle sizes capable of penetrating into the alveolar region of the lung, i.e., respirable-sized particles.[35] There were insufficient masses of materials collected in Stages 4 and 5 of the aerosol cyclone to perform the material characterization assays and free radical generation experiments for all study powders.

Characterization of Study Powders

The aerodynamically size-separated powders were characterized using scanning electron microscopy (SEM) to evaluate the morphology and size. Auger spectroscopy was used to determine surface elemental composition and particles were etched to a depth of 100 Å to evaluate changes in surface chemistry; X-ray diffraction (XRD) to identify crystalline constituents; helium pycnometry (Multipycnometer; Quantachrome Instruments, Boynton Beach, Fla.) to determine material density, and nitrogen gas adsorption (NOVA 2000e; Quantachrome) by the Brunauer, Emmett, and Teller (BET) method to determine specific surface area (SSA). Prior to measurement of surface area, all samples were outgassed for at least 3 hr at 150°C to 200°C under light vacuum (Flovac Degasser, P/N 05076; Quantachrome) to remove physisorbed compounds (e.g., water) from the powder surface. Estimates of surface area for each material were calculated according to the BET method from seven adsorption data points (relative pressures ranging from 0.03 to 0.30) using ultra-high purity nitrogen (cross-sectional area 16.2 $Å^2$) as the adsorbate. A minimum of four surface area measurements were performed on each sample. A commercially available α-alumina reference powder (BAM-PM-102; Bundesanstalt für Materialforschung und-prüfung; Berlin, Germany), with SSA of 5.41 $\pm$ 0.24 m^2/g, was analyzed in duplicate periodically throughout the study. The average measured SSA for the control sample, 5.63 $\pm$ 0.25 m^2/g, was within 4% of the certified value. Due to the small mass and low surface area of Stage 3 chamfer grinder powder, linear isotherms could not be obtained using nitrogen gas adsorption. As such, surface area of this size fraction of material was determined using krypton gas adsorption by a commercial laboratory.

Electron Spin Resonance (ESR) Studies

Our investigation concerns occupational exposures to cemented carbide particles. Since occupational exposures would involve reaction of the particles with macrophages and subsequent interaction with H_2O_2, we made the "Fenton-like" reaction our preliminary reaction of investigation. Thus, our primary focus was on reactions involving host defense. Production of free radicals by the size-separated powders was evaluated in cell-free and cellular reaction systems. The purpose of the cell-free tests was to understand production of free radicals by particles that contact lung and skin fluids, whereas the cellular test provided information on production of free radicals by particles that interact with lung cells.

Reagents

Phosphate-buffered saline (PBS) [KH_2PO_4 (1.06 mM), Na_2HPO_4 (5.6 mM), NaCl (154 mM), pH 7.4] was purchased from Biowhittaker Inc. (Walkersville, Md.). The PBS was treated with Chelex 100 purchased from Sigma Chemical Company (St. Louis, Mo.) to remove transition metal ion contaminants. Dulbecco's modified eagles medium (DMEM), 5,5-dimethyl-1-pyroline-oxide (DMPO), fetal bovine serum (FBS), $FeSO_4$, H_2O_2, and penicillin (10000 units/ml)/streptomycin (10 mg/mL) were purchased from Sigma Chemical Company. The DMPO spin trap was purified by charcoal decolorization and vacuum distillation and was free of ESR detectable impurities.

Cell Culture

RAW 264.7 mouse peritoneal monocytes were purchased from American Type Culture Collection (ATCC, Manassas, Va.). RAW 264.7 cells are commonly used and have been found to respond to particle exposure in a manner similar to primary alveolar macrophages.[36–41] RAW 264.7 cells were cultured in DMEM with 10% FBS, 2 mM L-glutamine, 100 units/mL penicillin and 0.1 mg/mL streptomycin at 37°C in a 5% CO_2 incubator. Cells were split after confluence approximately every 3 days.

Preparation of Study Powders

Each size fraction of each study powder was weighed, mixed with suspension fluid (PBS, artificial extracellular lung fluid, or artificial sweat solution), and vortexed for 10 s. The artificial extracellular lung fluid, herein referred to as surfactant, having pH 7.4, was prepared using the recipe given by Kanapilly et al.:[42] Na (0.1446 M), Ca (2×10^{-4} M), Cl (0.1275 M), PO_4 (1.2×10^{-3} M), SO_4 (2×10^{-4} M), glycine (5×10^{-3} M), cysteine (1.1×10^{-3} M), NH_3 (1.0×10^{-2} M), citrate (2.0×10^{-4} M), carbonate (2.7×10^{-2} M), and diethylenetriaminepentaacetic acid (2.0×10^{-4} M).

An artificial sweat solution was prepared with constituent concentrations that closely matched the median concentrations for human sweat summarized by Stefaniak and Harvey.[43] This artificial sweat contained 61 different constituents, including primary electrolytes, ionic constituents, organic acids and carbohydrates, amino acids, nitrogenous substances, and vitamins. The major constituents of this sweat solution were: Na (3.1×10^{-2}M), Cl (4.1×10^{-3} M), lactic acid (1.4×10^{-2} M), urea (1.0×10^{-2} M), and nicotinic acid (4.1×10^{-1} M). Each powder suspension was immediately pipetted into a reaction system (H_2O_2 or cellular).

Free Radical Measurements

ESR spin trapping was used to detect short-lived free radical intermediates. Hydroxyl radicals were measured using the addition-type reaction of a short-lived radical with a compound (spin trap) to form a relatively long-lived free radical product (spin adduct), which can then be studied using conventional ESR. Macrophages attack and engulf foreign bodies (including particles) that invade the lung where they can react with H_2O_2 as one of their defense mechanisms. This H_2O_2 can react with particles in a Fenton-like manner and generate more damaging free radicals.

Modeling this respiratory burst defense system with H_2O_2 and monocyte-macrophage cells provides a source of preliminary data on the biological reactivity of the particles involved.[44] Thus, powders were reacted with H_2O_2 in order to measure their potential to generate reactive radical species when inhaled and exposed to an organism's defense

systems.[45] For H_2O_2 Fenton-like reaction measurements,[46] reactants were mixed in test tubes at a final volume of 1.0 mL of PBS, surfactant, or artificial sweat in the presence of 0.1 mM H_2O_2 and 100 mM DMPO (final powder concentration of 1 mg/mL) and vortexed for 10 s. In this experimental system, a high dose was required to observe a reaction within the short exposure time necessitated by the use of ESR. Specifically, cells must be measured without the presence of media, serum, or sugars that can act as radical scavengers and therefore interfere with the reaction. As such, cells were reacted in the presence of PBS, DMPO, and study particles that enabled us to investigate generation of free radicals from various cemented carbide particles and compare differences between particle types.[39] The reaction mixture was then transferred to a flat cell for ESR measurement. Experiments were performed at room temperature, under ambient air.

For cellular measurements, reactants were mixed in test tubes at a final volume of 1.0 mL of 1×10^6/mL RAW 264.7 cells and 200 mM DMPO (final concentration of 5 mg powder/mL surfactant) and vortexed for 10 s. The cells were incubated for 3 min at 37°C then transferred to a flat cell for ESR measurement. Exposure to DMPO alone at a concentration of 200 mM for the short exposure time used has not shown cellular toxicity and does not cause generation of ROS.[47]

The intensity of the ESR signal was used to measure the amount of short-lived radicals trapped, and the hyperfine couplings of the spin adduct were characteristic of the original trapped radicals. Spin trapping was the method of choice for detection and identification of free radical generation due to its specificity and sensitivity. All ESR measurements were conducted using a Bruker EMX spectrometer (Bruker Instruments Inc. Billerica, Mass.) and a flat cell assembly. Hyperfine couplings were measured (to 0.1 G) directly from magnetic field separation using potassium tetraperoxochromate (K_3CrO_8) and 1,1-diphenyl-2-picrylhydrazyl as reference standards.[48,49] The relative radical concentration was estimated by multiplying half of the peak height by $(\Delta H_{pp})^2$, where ΔH_{pp} represents peak-to-peak width. The Acquisit program was used for data acquisitions and analyses (Bruker Instruments Inc.).

Statistics

Data were expressed as the mean ± standard error of the triplicate measures of each material in each group. One-way analysis of variance (ANOVA) models were used to investigate the fixed effects of particle size and powder type on ROS levels within a given test system (PC-SAS version 9.1). In these procedures, the Tukey's test option was specified for multiple comparisons. ANOVA F-statistics were used to note the overall differences in the means for ROS levels among the sizes and types of powder in a test system, while Tukey's test was used to identify specific paired differences between different means. Statistical significance was set at $p < 0.05$.

RESULTS

Characteristics of Study Powders

Figures 1 and 2 display representative SEM micrographs of the aerodynamically size-separated powders collected in Stage 3 of the aerosol cyclone ($D_{50} = 2.9$ μm). As expected, similar particle morphologies were observed in other micrographs for the corresponding size-separated powders of each material (data not shown). Post-sintered powder from the chamfer grinder consisted of particles that were relatively more compacted than precursor or pre-sintered materials as illustrated by the flattened face of the these particles, especially in the larger sizes (Figure 2c).

Table I summarizes the characteristics of the aerodynamically size-separated study materials. Analysis of particle composition using energy dispersive X-ray analysis demonstrated that elemental composition of the materials was consistent with the respective powder type.[27] Surfaces of tungsten metal, tungsten carbide, and cobalt powders were rich in oxygen, which suggests the presence of surface metal oxides. Admixture powder surfaces were rich in tungsten, carbon, and oxygen, with minor amounts of cobalt. Cobalt was not identified on the surfaces of pre-sintered powder from the spray dryer. Surfaces of post-sintered powders from the chamfer grinder contained tungsten, carbon, oxygen, and cobalt.

Analysis of crystalline composition by XRD revealed that the feedstock powders were homogeneous powders, whereas the process powders were heterogeneous. Within a given study powder, the predominant crystalline phase was the same regardless of aerodynamic particle size. Density values of feedstock powders were generally near theoretical values. Specific surface area varied by a factor of 15 among the various sizes of materials.

Free Radical Generation

Radicals Generated from H_2O_2 Reaction

Figure 3 is the standard presentation of representative spectra generated from (a) DMPO, (b) DMPO + H_2O_2, and (c) DMPO + H_2O_2+ tungsten carbide (1 mg powder/mL) powder suspended in PBS to create a Fenton-like reaction. The spectrum in Figure 3c illustrates 1:2:2:1 quartet splitting of $a_N = a_H = 14.9$ as indicated by the magnetic field legend. Using these splitting constants as well as verification with scavengers and chelators, this 1:2:2:1 quartet can be assigned to the DMPO/·OH adduct, showing ·OH radical generation by tungsten carbide. Chamfer grinder and spray dryer powders floated on PBS in the PBS plus H_2O_2 reaction system, precluding determination of radical generation. All other study powders readily went into suspension in this system; feedstock cobalt powder did not generate radicals.

ANOVA models indicated that, on a mass basis, average radical levels differed among study powders. From Tukey's multiple comparison tests, average ·OH radical generation levels were similar between tungsten and admixture powders; however, tungsten carbide was significantly lower ($p < 0.05$). Feedstock tungsten metal powder and tungsten carbide powder

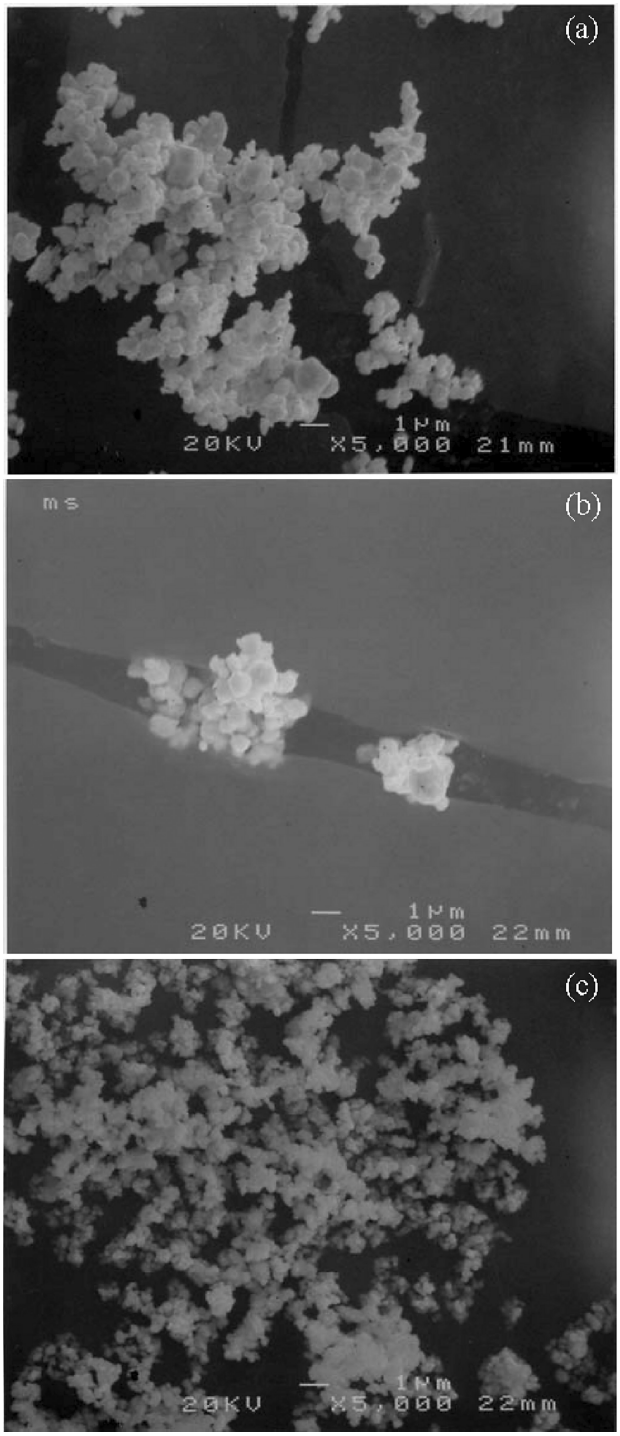

FIGURE 1. Representative scanning electron micrographs of aerodynamically size-separated study powders collected in stage 3 of the aerosol cyclone: (a) tungsten metal, (b) tungsten carbide, and (c) cobalt metal.

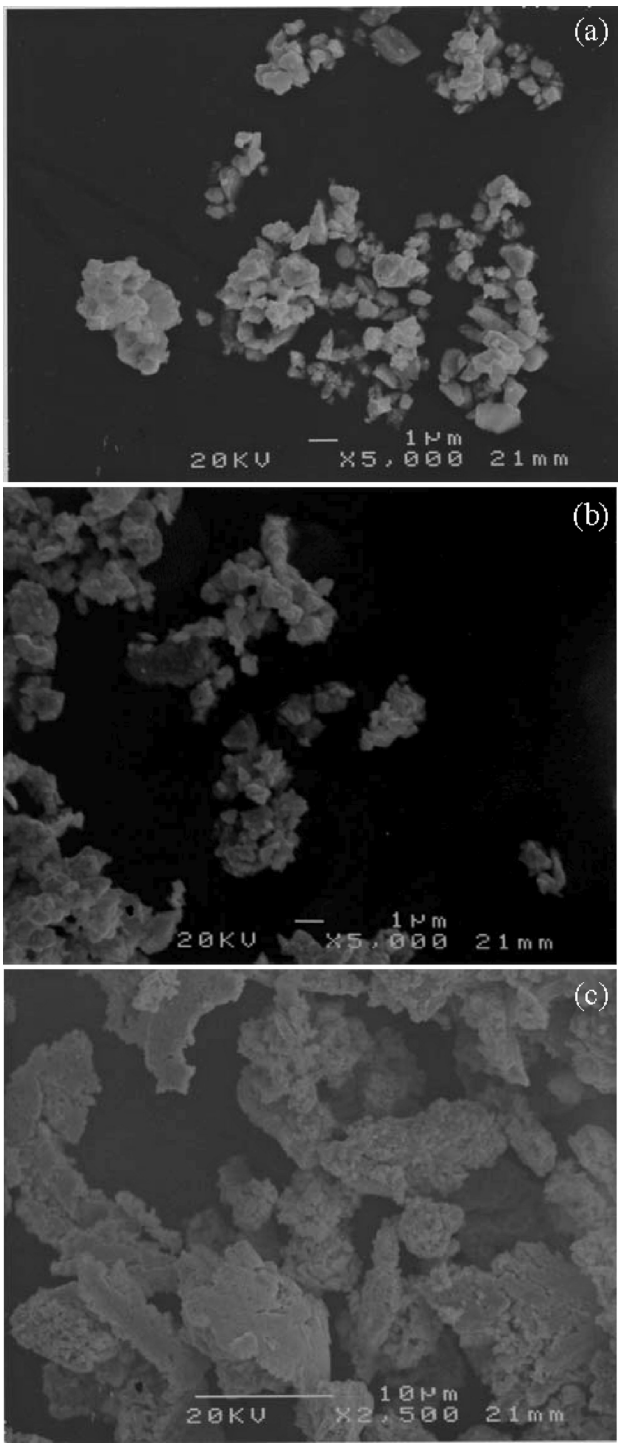

FIGURE 2. Representative scanning electron micrographs of aerodynamically size-separated process-sampled powders collected in stage 3 of the aerosol cyclone: (a) spray dryer and (b) chamfer grinder. The images illustrate that post-sintered chamfer grinder particles were relatively more compacted than feedstock or pre-sintered materials. Image (c) is stage 1 chamfer grinder particles and further highlights the compactness of these particles, especially at the larger sizes.

TABLE I. Physicochemical Properties of Aerodynamically Size-Separated Feedstock Powders, Process Intermediary Powders, and Post-Sintered Cemented Tungsten Carbide Powders

		Constituents[A]			
Powder	**D_{50} (μm)**	**Surface**	**Crystalline**	**Density (g/cm^3)**	**Surface Area (m^2/g)**
Tungsten	>10	O, W, C	W	18.9 ± 0.2	0.61 ± 0.04
	4.3	O, W, C	W	19.8 ± 0.3	0.87 ± 0.05
	2.9	O, W, C	W	18.9 ± 0.2	1.04 ± 0.11
Tungsten carbide	>10	O, W, C	WC, W_2C	15.1 ± 0.1	0.55 ± 0.02
	4.3	W, O, C	WC, W_2C	15.6 ± 0.1	0.65 ± 0.03
	2.9	O, W, C	WC, W_2C	14.8 ± 0.1	0.82 ± 0.06
Cobalt	>10	O, Co	Co	7.7 ± 0.0	6.05 ± 0.87
	4.3	O, Co	Co	7.6 ± 0.2	6.19 ± 0.61
	2.9	O, Co	Co	7.7 ± 0.1	6.02 ± 0.35
Admixture	>10	O, W, C, Co	WC, W_2C, Co	13.8 ± 0.1	0.74 ± 0.08
	4.3	O, W, C, Co	WC, W_2C, Co	14.4 ± 0.1	0.84 ± 0.10
	2.9	O, W, C, Co	WC, W_2C, Co	13.9 ± 0.1	1.14 ± 0.05
Spray dryer	>10	C	WC, W, W_2C, Co	10.4 ± 0.1	0.79 ± 0.09
	4.3	C	—	—	0.79 ± 0.11
	2.9	C, O	—	—	1.43 ± 0.08
Chamfer grinder	>10	C, O, W, Co	WC	12.9 ± 0.1	0.49 ± 0.07
	4.3	O, C, W, Co	—	—	0.61 ± 0.09
	2.9	C, O, W, Co	—	—	1.11 ± 0.05

Note: Dashes indicate insufficient mass of aerodynamically size-separated material available for this analysis.
[A]The order of constituents listed is from most to least abundant; O = oxygen, W = tungsten, C = carbon, Co = cobalt, WC = tungsten monocarbide, W_2C = ditungsten carbide.

and the admixture powder exhibited a trend of increased radical production with decreased particle size (data not shown). ANOVA models confirmed size-dependent differences in radical generation levels among powders. Tukey's tests revealed that radical generation levels differed among Stage 1 ($p < 0.05$) and Stage 2 ($p < 0.05$) powders, whereas Stage 3 tungsten carbide generated lower levels ($p < 0.05$) of radicals than tungsten metal or the admixture.

When radical generation levels were normalized to dose expressed as powder surface area, results became more similar among sizes of a given powder. ANOVA models indicated area-dependent differences in radical generation between powders. Notably, Stage 3 admixture and tungsten particles generated higher ($p < 0.05$) levels of radicals than tungsten carbide (data not shown).

Figure 4 summarizes the results from the reaction of each study powder with H_2O_2 (0.1 mM), in the presence of DMPO (100 mM) while suspended in an artificial extracellular lung surfactant (1 mg powder/mL). ANOVA models indicated that on a mass basis (Figure 4a), average radical generation levels differed among study powders. Tukey's multiple comparison tests determined that radical generation levels were similar between tungsten and chamfer grinder powders ($p = 0.28$) but higher than all other powders ($p < 0.05$); i.e., tungsten ≈ chamfer grinder > tungsten carbide ≈ cobalt ≈ admixture ≈ spray dryer. Tungsten metal, tungsten carbide, and admixture exhibited lower overall ·OH radical signal strength in the surfactant plus H_2O_2 reaction system than in the PBS plus H_2O_2 system (data not shown).

ANOVA analysis confirmed size-dependent radical production among study powders in the surfactant plus H_2O_2 reaction system. Tukey's tests revealed that all sizes of tungsten and chamfer grinder powder generated higher levels ($p < 0.05$) of radicals than the corresponding sizes of tungsten carbide, cobalt, admixture, and spray dryer powders. In addition, Stages 2 and 3 admixture powder generated higher ($p < 0.05$) levels of radicals than cobalt or tungsten carbide alone. Note that the ESR data plotted in Figure 4a was normalized to total powder mass, not the mass of the tungsten carbide or cobalt in a powder. For a given powder, XRD analysis determined that the mass of tungsten carbide and/or cobalt varied little among aerodynamic size fractions (Table I). As such, normalizing the ESR data to tungsten carbide or cobalt mass only shifted the response to each powder proportionally higher but did not change the observed trends and conclusions (data not shown).

Thus, for the purpose of presentation in Figures 4a, 5a, and 6a the ESR data were normalized to total powder mass rather than individual constituent mass. As displayed in Figure 4b, when dose was expressed using total powder surface area as the dose metric, radical generation of each material became more similar among sizes of a given powder, but area-dependent differences existed between powder types. On a surface area basis, Stages 1, 2, and 3 tungsten and chamfer grinder powder generated higher levels ($p < 0.05$)

FIGURE 3. Example ESR spectra illustrating the generation of short-lived ·OH radicals by WC in PBS on reaction with H_2O_2: (a) DMPO, (b) DMPO + H_2O_2, and (c) DMPO + H_2O_2+ WC (1 mg powder/mL). The x-axis is the magnetic field in gauss (G) and the y-axis is peak intensity. ESR spectra were recorded 3 min after reaction was initiated in PBS (pH 7.4) containing H_2O_2 (0.1 mM) and DMPO (100 mM) vortexed for 10 s. For all cell-free experiments the ESR settings were: center field, 3480 G; scan width, 100 G; time constant, 0.40 sec; modulation amplitude, 1 G; receiver gain, 6.32×10^4; frequency, 9.828 GHz; and power, 20 mW.

of radicals than the corresponding stages of tungsten carbide, cobalt, admixture, and spray dryer powders. Stages 1, 2, and 3 admixture powder generated similar levels of radicals compared with tungsten carbide but higher ($p < 0.05$) levels of radicals compared to cobalt.

Figure 5 summarizes the results from the reaction of each study powder with H_2O_2 (0.1 mM) and DMPO (100 mM) while suspended in an artificial sweat solution (1 mg powder/mL). Radical generation levels in artificial sweat plus H_2O_2 were generally higher than observed in the surfactant reaction system. From ANOVA models followed by Tukey's tests, the relative ranking of powders from highest to lowest average radical generation in the sweat system (Figure 5a) was: cobalt metal > chamfer grinder > tungsten carbide > spray dryer > tungsten metal ≈ admixture; differences were statistically significant ($p < 0.05$). On a mass basis, powders exhibited a slight trend of increased radical production as particle size decreased.

ANOVA models revealed that radical generation levels differed among sizes of the different powder types, and Tukey's tests revealed that these differences followed the same general trend as reported for the average levels. When dose was normalized to powder surface area as the metric, radical generation levels within a given powder type generally became less dependent on particle size (Figure 5b), but area-dependent differences were observed among powder types. The heterogeneous chamfer grinder powder had lower surface area but radical generation per unit area was highest among powders. There was no difference in average radical generation levels between tungsten carbide and chamfer grinder powders ($p = 0.11$).

Cellular OH Radical Generation

Figure 6 summarizes observed radical generation for powders suspended in surfactant and exposed to the RAW 264.7 cell line. Cobalt metal powder did not generate radicals in the cellular system. ANOVA models revealed differences in average radical generation levels among powders (Figure 6a), with the ranking from highest to lowest being: chamfer grinder > tungsten ≈ spray dryer > tungsten carbide ≈ admixture; differences were significant ($p < 0.05$).

ANOVA models followed by Tukey's tests determined that all powders in the RAW 264.7 cell line reaction system exhibited a trend of increased radical production with decreased particle size. Powder size-specific radical generation levels followed the same trend as reported for the average levels. When dose was expressed as powder surface area (Figure 6b), radical generation levels within a given powder were nearly independent of particle size. Among powders, area-dependent differences existed. Notably, radical generation levels were highest for chamfer grinder material.

DISCUSSION

Among all reaction systems, the heterogeneous sintered chamfer grinder powder tended to produce higher levels of free radicals than any other individual study powder. Aside from the chamfer grinder powder, there was no clear trend across all reaction systems in production of free radicals by any other study powder. These observations suggest that production of free radicals by powders encountered during the manufacture of cemented tungsten carbides depends not only on the material surface chemistry but also the biological liquid media encountered upon deposition in the lung or on the skin, i.e., hazard potential is variable.

Role of Particle Physicochemical Properties in Generation of Free Radicals

Disconnect often exists between study materials used in laboratory toxicology studies and workplace exposure particle characteristics. In the current study, pre-sintered admixture and spray dryer materials generated low levels of ROS, although levels for the admixture tended to be higher than cobalt or tungsten carbide alone. For pre-sintered materials held in contact by weak electrostatic bonds or van der Waals forces, radical generation may be limited by the physical proximity of cobalt and tungsten carbide reactants on the surfaces of particles.

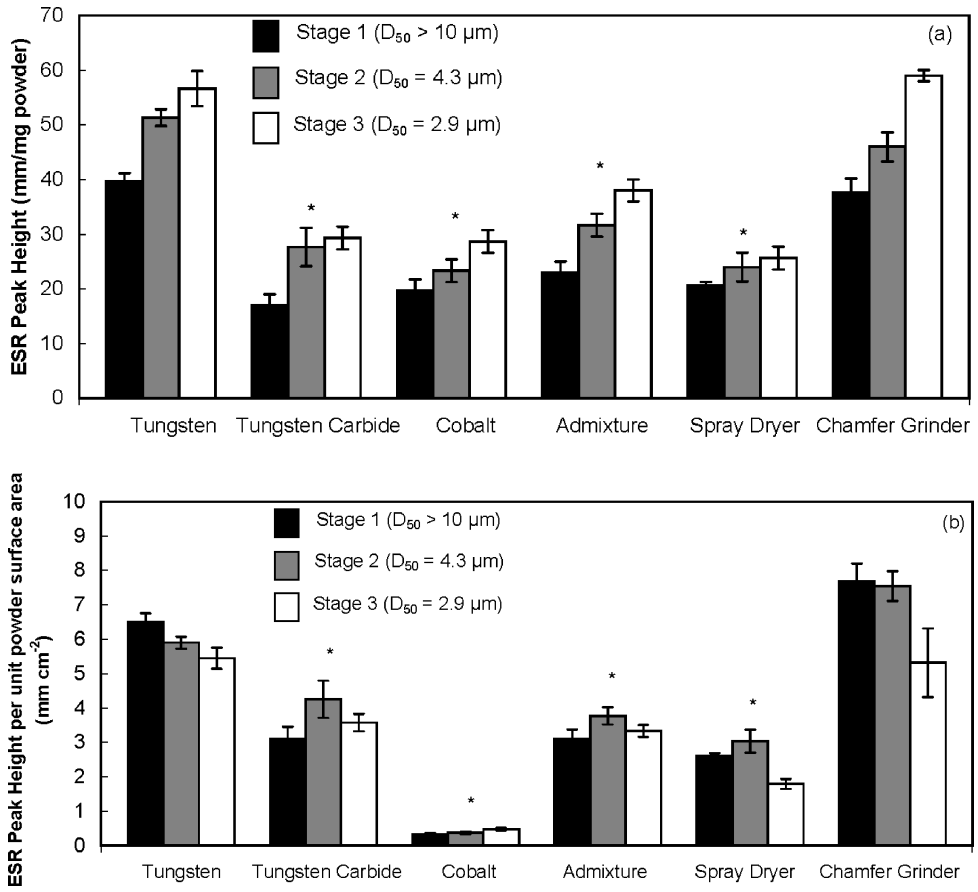

FIGURE 4. Plot of electron spin resonance (ESR) peak height for feedstock and process sampled powders collected at a cemented tungsten carbide manufacturer (1 mg powder/mL artificial lung surfactant) with H_2O_2 (0.1 mM) in the presence of DMPO (100 mM): (a) on a mass basis all study powders exhibited a similar trend of radical production increasing as particle size decreased, and (b) when dose was normalized to powder surface area, size-dependent differences in radical generation became less apparent in each powder. There was no difference in average ·OH radical generation level between tungsten metal powder and chamfer grinder powder ($p = 0.28$); * = average ·OH radical generation level of powder was significantly lower ($p < 0.05$) than tungsten metal powder or chamfer grinder powder. $n = 3$.

Among all study powders, post-sintered chamfer grinder particles generated the highest level of radicals in the surfactant plus H_2O_2 reaction system and the RAW 264.7 cellular reaction system. During sintering, the Co and WC powders densify (Figures 1 and 2) to form CTC alloy or "hard metal."[32] Thus, the elevated capacity of chamfer grinder particles to produce free radicals may be due to the intimate (chemically bonded) cobalt metal/carbide contact on the surfaces of this alloy material, which enhances transfer of electrons from cobalt metal to the carbide.

Particle surface characteristics are known to control the biological activity of many inhaled poorly soluble particles, including manganese dioxide,[50] titanium dioxide,[51] and pathogenic mineral dusts such as crystalline silica.[30] Previous studies of ROS generation by carbide materials normalized exposures to the total mass of bulk cobalt added to a reaction system.[20,21] In these studies, "4-μm extrafine" cobalt particles were used as a test material; assuming compact spherical shape, the surface 100 Å layer of this size particle would account for only 0.075% of the total mass with the remainder inaccessible to contact with tungsten carbide until the surface layer dissolved to expose the underlying cobalt. Additionally, the radical generation levels observed in these studies were enhanced by the presence of tungsten carbide. Thus, total mass of cobalt may not be a toxicologically relevant exposure metric for ROS generated on surfaces of cemented carbide dusts. Going beyond mass, when ROS levels were normalized to total available particle surface area, results from our experiments indicated that levels become more similar among the three fractions of a study powder as shown in Figures 4b, 5b, and 6b.

In our study, both chamfer grinder and admixture powders tended to generate higher levels of radicals on a surface area basis than feedstock cobalt or tungsten carbide powders alone. The observed similarity in ROS levels among size fractions of a material supports the premise that contact between cobalt and tungsten carbide is necessary;[20] however, higher levels of radical production by heterogeneous powders suggests that the mechanism of radical generation was dependent upon both particle surface area and surface chemistry. Total available

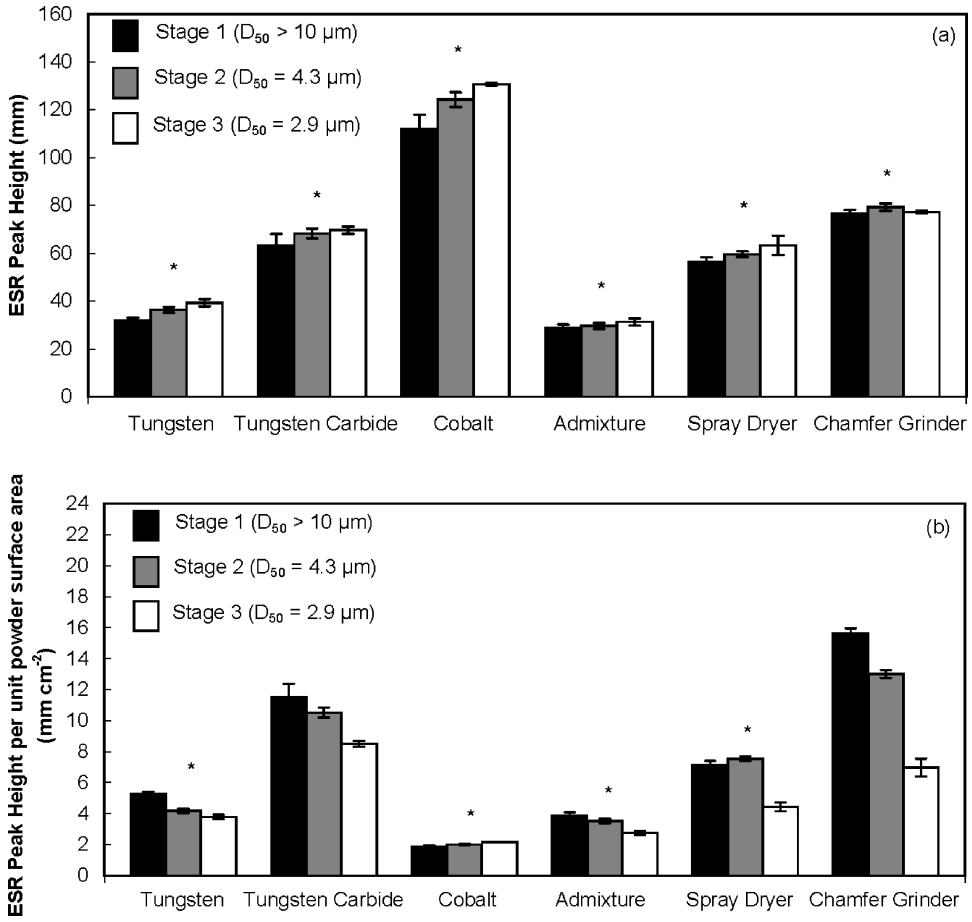

FIGURE 5. Plot of electron spin resonance (ESR) peak height for feedstock and process sampled powders collected at a cemented tungsten carbide manufacturer (1 mg powder/mL artificial sweat solution) with H_2O_2 (0.1 mM) in the presence of DMPO (100 mM): (a) on a mass basis all study powders exhibited only a slight trend of radical production increasing as particle size decreased, * = average ·OH radical generation level of powder was significantly different from all other study powders ($p < 0.05$); (b) on a surface area basis radical production was generally independent of particle size, no difference was observed in average ·OH radical levels between tungsten carbide and chamfer grinder powders ($p = 0.10$) and * = average ·OH radical generation level of powder was significantly lower ($p < 0.05$) than tungsten carbide powder or chamfer grinder powder. n = 3.

surface area accounted for a portion of ROS levels generated by the heterogeneous process-sampled chamfer grinder particles as indicated by the decrease in radical generation levels with increasing available surface area.

A similar trend was noted for the heterogeneous spray dryer material. Measures of surface area by gas adsorption are not chemical specific, as such, for materials with heterogeneous surface chemistry such as spray dryer or chamfer grinder particles, the fraction of available surface that was tungsten carbide or cobalt appears to be less than the total. The remaining surface area may be due impurities, e.g., inert fine diamond dust from the grinding used for chamfer grinding. As such, the observed trend in radical generation for chamfer grinder material indicated that ROS levels were limited to the biologically active fraction of the surface, i.e., the portion of surface area containing surface cobalt and tungsten carbide molecules in contact.

For mixtures of discrete tungsten carbide and cobalt (e.g., admixture) the biologically active surface area is the portion of cobalt particle surface area and the portion of tungsten carbide particle surface area that are in contact. Cobalt is known to be more soluble than tungsten carbide in lung fluids.[52] Thus, to support development of HMD, a consistent cobalt lung burden is necessary to maintain chronic biological production of ROS with highly biopersistent tungsten carbide that is retained in the lung over a period of time sufficient to develop fibrosis.[7]

Hard Metal Disease

Radical generation in tissue is a normal part of cellular respiration; however, an imbalance between radical generation and radical scavenging may result in damage to the organism. Particles can be phagocytized by cells and can accumulate within vacuoles in the cytoplasm.[53] This internalization has been associated with the cellular stress response to

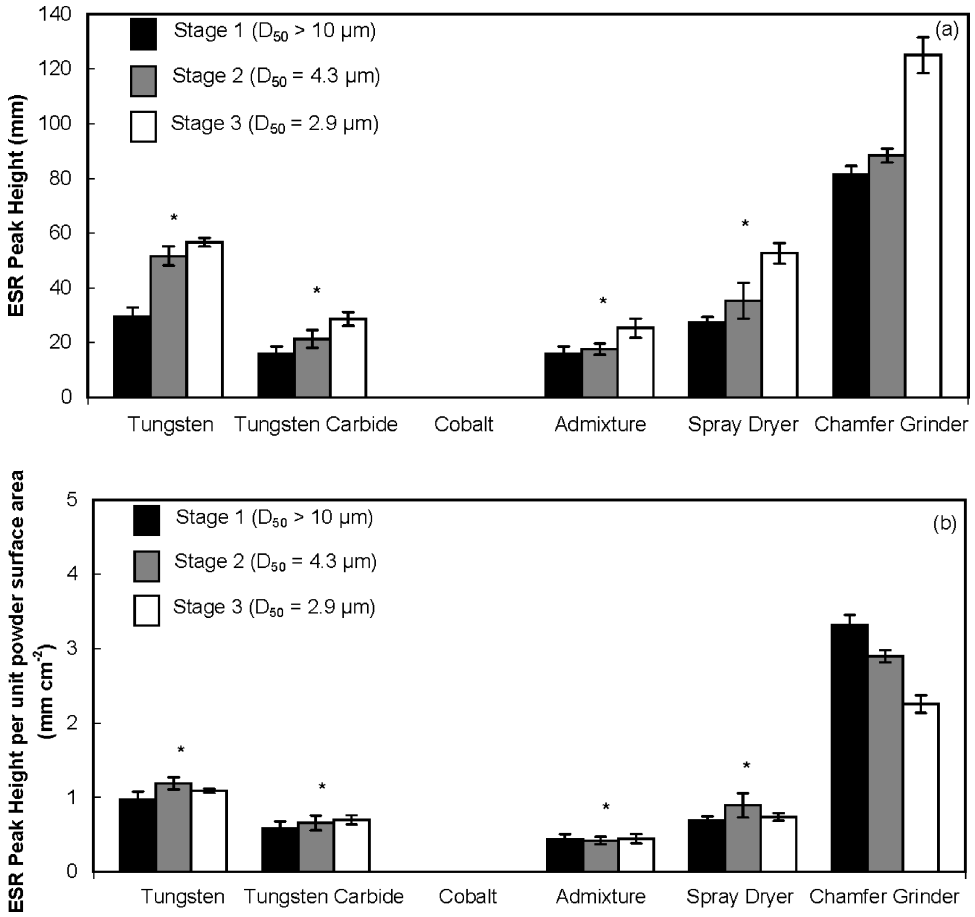

FIGURE 6. Plot of electron spin resonance (ESR) peak height for feedstock and process sampled powders collected at a cemented tungsten carbide manufacturer (5 mg powder/mL surfactant) with RAW 264.7 cells (1×10^6/mL) in the presence of DMPO (200 mM). For the cellular experiments ESR settings were: center field, 3488 G; scan width, 100 G; time constant, 0.40 s; modulation amplitude, 1 G; receiver gain, 6.32×10^4; frequency, 9.828 GHz; and power, 60 mW. (a) on a mass basis all powders except cobalt metal (did not generate radicals) exhibited a trend of increased radical production with decreased particle size with radical generation highest for the chamfer grinder higher in this system than any other system tested in this study, (b) on a surface area basis radical production was generally independent of particle size. * = average ·OH generation level was significantly lower ($p < 0.05$) than chamfer grinder powder. n = 3.

particle exposure.[54] These particles can result in the chronic production of ROS that may lead to DNA damage and lipid peroxidation,[54] activation of nuclear transcription factors (NF-κB, AP-1),[55] apoptosis,[56] and activation of mitogen-activated protein (MAP) kinases,[55] as well as further downstream activations of biological signaling pathways.

The observed role of surface chemistry in the radical generation capacity of powders encountered during the production of cemented carbides has critical implications for exposure assessment for HMD. Historically, exposures of cemented carbide manufacturing workers were measured as total airborne cobalt aerosol mass concentration using 37-mm cassette samplers without regard to particle size despite the fact that workers are exposed to a range of cobalt- and tungsten-containing particle sizes.[27,28] Large particles (aerodynamic diameter greater than 10 μm) deposit in the ciliated upper and conducting airways where they are rapidly cleared by mechanical clearance. Small particles (aerodynamic diameter less than 4 μm) such as those from Stages 2 and 3 of the aerosol cyclone used in this study will deposit in the nonciliated alveolar region of the lung and are cleared more slowly by macrophages or chemical dissolution.

In our study, Stages 2 and 3 chamfer grinder and admixture powders tended to generate higher levels of radicals than corresponding fractions of feedstock cobalt or tungsten carbide powders alone. If HMD is caused by generation of ROS by cobalt-tungsten carbide particle mixtures[22,23] that deposit in the alveolar region of the lung, then a respirable exposure metric for both metals is likely biologically appropriate.[28] This metric consists of a physical exposure material component (particle size capable of depositing in the alveolar region of the lung and corresponding particle surface area) and a chemical exposure material component (biologically active particle surface chemistry capable of generating free radicals).

Allergic Contact Dermatitis

Van den Broeke et al.[26] reported that ascorbic acid (2 mM), a known antioxidant, inhibited ionic (Co^{+2})-mediated free radical generation in PBS solutions. In our study, cobalt metal powder did not generate ·OH radicals in the PBS plus H_2O_2 reaction system (data not shown). However, on a mass basis cobalt metal powder generated significantly more ·OH radicals than any other study powder in the artificial sweat plus H_2O_2 reaction system. The artificial sweat used in our H_2O_2 reaction system contained 0.01 mM ascorbic acid, which is a factor of 20 times lower than used by Van den Broeke et al.;[26] however, inhibition of radical generation in the sweat plus H_2O_2 reaction system cannot be ruled out.

Workers engaged in the manufacture of cemented tungsten carbides may accumulate several milligrams of cobalt on their hands.[29] With regards to ACD, generation of ·OH radicals by milligram quantities of cobalt powder in an artificial sweat plus H_2O_2 reaction system supports the plausibility of radical generation on the skin stratum corneum. Whether radical generation and potential alteration of biomolecules to form hapten[26] occurs in the underlying immunologically active epidermis skin layer could not be elucidated from our data and remains poorly understood.

CONCLUSIONS

Workers engaged in the manufacture of CTC may be exposed to Co, W, WC, and mixtures of these metals. In this study, industrial powders sampled from a cemented carbide manufacturer generated ·OH radicals in test systems intended to mimic exposure via inhalation and skin contact. If an imbalance between radical generation and radical scavenging occurs in tissue it may stimulate inflammation, which could result in damage to surrounding cells. For the industrial powders evaluated in this study, levels of free radical generation were dependent on the biologically active fraction of total powder surface area. The implication of these data for HMD is that exposure assessment efforts should account for both airborne particle physical (i.e., respirable, surface area) and chemical (i.e., biologically active particle surface chemistry) properties. Generation of ·OH radicals by study powders in an artificial sweat model supports, in concept, the biological plausibility for involvement of cobalt-mediated redox reactions in development of ACD. Efforts to minimize inhalation and skin contact with dusts generated during production of CTC are prudent.

ACKNOWLEDGMENTS

The authors thank D. Sbarra at NIOSH for technical assistance and N. Edwards at NIOSH for development of the figures. The authors also thank M.A. Virji and M. Rao at NIOSH for critical review of this manuscript.

REFERENCES

1. **Santhanam, A.T.:** Cemented carbides. In *Kirk-Othmer Encyclopedia of Chemical Technology*, *4th Edition, Vol. 4, Bearing Materials to Carbon*. M. Howe-Grant (ed.). New York: Wiley-Interscience, 1992. pp. 848–860.
2. **Meyer-Bisch, C., Q.T. Pham, J.-M. Mur, et al.:** Respiratory hazards in hard metal workers: A cross sectional study. *Br. J. Ind. Med. 46*:302–309 (1989).
3. **Spince, N.L., R.I. Chamberlin, C.A. Hales, A.L. Weber, and H. Kazemi:** Respiratory disease in tungsten carbide production workers. *Chest 86*:549–557 (1984).
4. **Sprince, N.L., L.C. Oliver, E.A. Eisen, R.E. Greene, and R.I. Chamberlin:** Cobalt exposure and lung disease in tungsten carbide production. *Am. Rev. Respir. Dis. 138*:1220–1226 (1988).
5. **Cugell, D.W., W.K.C. Morgan, D.G. Perkins, and A. Rubin:** The respiratory effects of cobalt. *Arch. Intern. Med. 150*:177–183 (1990).
6. **Fischbein, A., J.-C.J. Luo, S.J. Solomon, S. Horowitz, W. Hailoo, and A. Miller:** Clinical findings among hard metal workers. *Br. J. Ind. Med. 49*:17–24 (1992).
7. **Moriyama, H., M. Kobayashi, T. Takada, et al.:** Two-dimensional analysis of elements and mononuclear cells in hard metal lung disease. *Am. J. Resp. Crit. Care Med. 176*:70–77 (2007).
8. **Santos, R., and A. Goossens:** An update on airborne contact dermatitis: 2001–2006. *Contact Dermatitis 57*:353–360 (2007).
9. **Buzard, G.S., and K.S. Kasprzak:** Possible roles of nitric oxide and redox cell signalling in metal-induced toxicity and carcinogenesis: A review. *J. Environ. Pathol. Toxicol. Oncol. 19*:179–199 (2000).
10. **Wang, S., and X. Shi:** Molecular mechanisms of metal toxicity and carcinogenesis. *Mol. Cell. Biochem. 222*:3–9 (2001).
11. **Chen, F., and X. Shi:** Signaling from toxic metals to NF-kappaB and beyond: Not just a matter of reactive oxygen species. *Environ. Health Perspect. 110 (Suppl 5)*:807–811 (2002).
12. **Ding, M., and X. Shi:** Molecular mechanism of Cr(VI)-induced carcinogenesis. *Mol. Cell. Biochem. 234/235*:293–300 (2002).
13. **Harris, G.K., and X. Shi:** Signaling by carcinogenic metals and metal-induced reactive oxygen species. *Mutat. Res. 533*:183–200 (2003).
14. **Qian, Y., V. Castranova, and X. Shi:** New perspectives in arsenic-induced cell signal transduction. *J. Inorg. Biochem. 96*:271–278 (2003).
15. **Leonard, S.S., J.J. Bower, and X. Shi:** Metal-induced toxicity and carcinogenesis, mechanisms and cellular responses. *Mol. Cell. Biochem. 255*:3–10 (2004).
16. **Chen, F., and X. Shi:** Intracellular signal transduction of cells in response to carcinogenic metals. *Crit. Rev. Oncol. Hematol. 42*:105–121 (2002).
17. **Halliwell, B., and J.M.C. Gutteridge:** Oxygen toxicity, oxygen radicals, transition metals, and disease. *J. Biochem. 219*:1–14 (1984).
18. **Ho, Y.S., J.L. Magnenat, M. Gargano, and J. Cao:** The nature of antioxidant defense mechanisms: A lesson from transgenic studies. *Environ. Health Perspect. 106(Suppl.)*:1219–1228 (1998).
19. **Shi, X., A. Chiu, C.T. Chen, B. Halliwell, V. Castranova, and V.J. Vallyathan:** Reduction of chromium(VI) and its relationship to carcinogenesis. *J. Toxicol. Environ. Health. 2*:101–118 (1998).
20. **Lison, D., P. Carbonnelle, L. Mollo, R. Lauwerys, and B. Fubini:** Physicochemical mechanism of the interaction between cobalt metal and carbide particles to generate toxic activated oxygen species. *Chem. Res. Toxicol. 8*:600–606 (1995).
21. **Zanetti, G., and B. Fubini:** Surface interactions between metallic cobalt and tungsten carbide particles as a primary cause of hard metal disease. *J. Mater. Chem. 7*:1647–1654 (1997).
22. **Bennett, L.H., J.R. Cuthill, A.J. McAlister, N.E. Erickson, and R.E. Watson:** Electronic structure and catalytic behavior of tungsten carbide. *Science 184*:563–565 (1974).
23. **Goebeler, M., G. Meinardus-Hager, J. Roth, S. Goerdt, and C. Sorg:** Nickel chloride and cobalt chloride, two common contact sensitizers, directly induce expression of intercellular adhesion molecule-1 (ICAM-1), vascular cell adhesion molecule-1 (VCAM-1), and endothelial leukocyte adhesion molecule (ELAM-1) by endothelial cells. *J. Invest. Dermatol. 100*:759–765 (1993).

24. **Goebeler, M., J. Roth, E.B. Bröcker, C. Sorg, and K. Schulze-Osthoff:** Activation of nuclear factor-kappa B and gene expression in human endothelial cells by the common haptens nickel and cobalt. *J. Immunol. 155*:2459–2467 (1995).
25. **Forte, G., F. Petrucci, and B. Bocca:** Metal allergens of growing significance: Epidemiology, immunotoxicology, strategies for testing and prevention. *Inflamm. Allergy Drug Targets 7*:145–162 (2008).
26. **Van den Broeke, L.T., A. Gräslund, J.L.G. Nilsson, J. Wahlberg, A. Scheynius, and A.T. Karlberg:** Free radicals as potential mediators of metal allergy: Ni^{+2}- and Co^{+2}- mediated free radical generation. *Eur. J. Pharm. Sci. 6*:279–286 (1998).
27. **Stefaniak, A.B., G.A. Day, C.J. Harvey, et al.:** Characteristics of dusts encountered during the production of cemented tungsten carbides. *Ind. Health. 45*:793–803 (2007).
28. **Stefaniak, A.B., M.A. Virji, and G.A. Day:** Characterization of exposures among cemented tungsten carbide workers. Part I: Size-fractionated exposures to airborne cobalt and tungsten particles. *J. Expo. Sci. Environ. Epidemiol. 19*:475–491 (2009).
29. **Day, G.A., M.A, Virji, and A.B. Stefaniak:** Characterization of exposures among cemented tungsten carbide workers. Part II: Assessment of surface contamination and skin exposures to cobalt, chromium and nickel. *J. Expo. Sci. Environ. Epidemiol. 19*:423–434 (2009).
30. **Fubini B.:** Surface reactivity in the pathogenic response to particulates. *Environ. Health Perspect. 105 (Suppl 5)*:1013–1020 (1997).
31. **Oberdörster, G., A. Maynard, K. Donaldson, et al.:** Principles for characterizing the potential human health effects from exposure to nanomaterials: Elements of a screening strategy. *Part. Fibre Toxicol. 2*:8 (2005).
32. **Brookes, K.J.A.:** *Cemented Carbides for Engineers and Tool Users*. East Barnet, UK: International Carbide Data, 1983. pp. 1–19.
33. **Smith, W.B., R.R. Wilson, and D.B. Harris:** A five-stage cyclone system for in situ sampling. *Environ. Sci. Technol. 13*:1387–1392 (1979).
34. **Hoover, M.D., B.T. Castorina, G.L. Finch, and S.J. Rothenberg:** Determination of the oxide layer thickness on beryllium metal particles. *Am. Ind. Hyg. Assoc. J. 50*:550–553 (1989).
35. **Lippman, M.:** Particle size-selective sampling for particulate air contaminants. In *Rationale for Particle Size-Selective Aerosol Sampling*, J.H. Vincent (ed.). Cincinnati, Ohio: ACGIH, 1999. p. 18.
36. **Hiura, T.S., M.P. Kaszubowski, N. Li, and A.E. Nel:** Chemicals in diesel exhaust particles generate reactive oxygen radicals and induce apoptosis in macrophages. *J. Immunol. 163*:5582–5591 (1999).
37. **Jalava, P.I., O. Raimo, A.I. Halinen, et al.:** In vitro inflammation and cytotoxic effects of size-segregated particulate samples collected during long-range transport of wildfire smoke to Helsinki. *Toxicol. Appl. Pharmacol. 215*:341–353 (2006).
38. **Leonard, S.S., S. Wang, X. Shi, B.S. Jordan, V. Castranova, and M.A. Dubick:** Wood smoke particles generate free radicals and cause lipid peroxidation, DNA damage, NF-κB activation and TNF-α release in macrophages. *Toxicology 150*:147–157 (2000).
39. **Leonard, S.S., J.R. Roberts, J.M. Antonini, V. Castranova, and X. Shi:** $PbCrO_4$ mediates cellular responses via reactive oxygen species. *Mol. Cell Biochem. 255*:171–179 (2004).
40. **Li, N., C. Sioutas, A. Cho, et al.:** Ultrafine particulate pollutants induce oxidative stress and mitochondrial damage. *Environ. Health Perspect. 111*:455–460 (2003).
41. **Zhang, Y., C.C. Fong, M.S. Wong, et al.:** Molecular mechanisms of survival and apoptosis in RAW 264.7 macrophages under oxidative stress. *Apoptosis 10*:545–556 (2005).
42. **Kanapilly, G.M., O.G. Raabe, C.H.T. Go, and R.A. Chimenti:** Measurement of in vitro dissolution of aerosol particles for comparison to in vivo dissolution in the lower respiratory tract after inhalation. *Health Phys. 24*:497–507 (1973).
43. **Stefaniak, A.B., and C.J. Harvey:** Dissolution of materials in artificial skin surface film liquids. *Toxicol. In Vitro 20*:1265–1283 (2006).
44. **Dahlgren, C., A. Karlsson, and J. Bylund:** Measurement of respiratory burst products generated by professional phagocytes. *Methods Mol. Biol. 412*:349–363 (2007).
45. **Halliwell, B., and J.M.C. Gutteridge:** *Oxidative Stress: Free Radicals in Biology and Medicine, 4th edition*. New York: Oxford University Press, 2007. pp. 79–100, 405–417.
46. **Fenton, H.J.H:** Oxidation of tartaric acid in presence of iron. *J. Chem. Soc. Trans. 65*:899–911 (1894).
47. **Haseloff, R.F., K. Mertsch, E. Rohde, I. Baeger, I.A. Grigor'ev, and I.E. Blasig:** Cytotoxicity of spin trapping compounds. *FEBS Lett. 418*:73–75 (1997).
48. **Buettner, G.R.:** ESR parameters of spin adducts. *Free Radic. Biol. Med. 3*:259–303 (1987).
49. **Janzen, E.G., and B.J. Blackburn:** Detection and identification of short-lived free radicals by an electron spin resonance trapping technique. *J. Am. Chem. Soc. 90*:5909–5910 (1968).
50. **Lison, D., C. Lardot, F. Huaux, G. Zanetti, and B. Fubini:** Influence of particle surface area on the toxicity of insoluble manganese dioxide dusts. *Arch. Toxicol. 71*:725–729 (1997).
51. **Oberdörster, G., J. Ferin, and B.E. Lehnert:** Correlation between particle size, in vivo particle persistence, and lung injury. *Environ. Health Perspect. 102 (Suppl 5)*:173–179 (1994).
52. **Edel, J., E. Sabbioni, R. Pietra, et al.:** Trace metal lung disease: In vitro interaction of hard metals with human lung and plasma components. *Sci. Total Environ. 95*:107–117 (1990).
53. **Sidhu, M.K., C. Fernandez, M.Y. Khan, S. Kumar:** Induction of morphological transformation, anchorage-independent growth and plasminogen activators in non-tumorigenic human osteosarcoma cells by lead chromate. *Anticancer Res. 11*:1045–1053 (1991).
54. **Shi, X., Y. Mao, A.D. Knapton, et al.:** Reaction of Cr(VI) with ascorbate and hydrogen peroxide generates hydroxyl radicals and causes DNA damage: Role of a Cr(IV)-mediated Fenton-like reaction. *Carcinogenesis 15*:2475–2478 (1994).
55. **Chen, F., M. Ding, Y. Lu, et al.:** Participation of MAP kinase p38 and IkappaB kinase in chromium (VI)-induced NF-kappaB and AP-1 activation. *J. Environ. Pathol. Toxicol. Oncol. 19*:231–238 (2000).
56. **Ye, J., S. Wang, S.S. Leonard, et al.:** Role of reactive oxygen species and p53 in chromium(VI)-induced apoptosis. *J. Biol. Chem. 274*:34974–34980 (1999).